

## Fluences and Spectra of Accelerator Generated Fast Neutrons

Gunter H.R. Kegel, Peter F. Bertone, Diane L. Case, David J. DeSimone,  
Causon K.C. Jen, Chandrika Narayan, Michael O'Connor and Parrish Staples.

Radiation Laboratory  
University of Massachusetts - Lowell  
Lowell, Massachusetts 01854.

### Abstract

A fast neutron irradiation station has been designed at the University of Massachusetts - Lowell. The fluence delivered by this station is less than that of a nuclear reactor but it is essentially free of slow neutrons and the admixture of gamma rays is small. We describe the station, dosimetry methods, a computer code, verification techniques and applications. The information we provide should enable others to construct a similar station on their type CN or tandem accelerators.

### I. INTRODUCTION

Neutron scattering studies in the MeV-region have been performed at Lowell in the past 25 years. In much of this work neutrons were generated by irradiating a thin metallic lithium target with protons produced by the Lowell 5.5 MV, type CN Van de Graaff accelerator. For the purpose of obtaining a neutron spectrum, which covers in a continuous form fast neutron energies from zero to 3 MeV, we started using thick metallic lithium targets in 1983. These thick targets have not yet been used in our neutron scattering work, but they have found application in a variety of studies. We estimate that, to this date, about 100 thick lithium targets have been used with a total run time in excess of 1000 hours. It seems, at this writing, that the technique and associated procedures have matured and that our experience should be reported to a wider audience.

Applications of our neutron source cover a broad spectrum. Most work involved radiation damage studies in electronic devices, but it also included investigations of optical devices, irradiation of living biota, such as bacteria and seeds, and of dead specimens, e.g. bone. Our fast neutron source does not have the same fluence as a nuclear reactor, it generates about  $6.2 \times 10^{10}$  neutrons/s or about as

much as 1 W (thermal) reactor or as much as a 25 Ci californium source. This source would cost close to  $\$2 \times 10^6$ , not including shielding and handling equipment.

Some users prefer our fast neutron station to a reactor because they see one or the other of the following advantages: (i) The small number of gamma rays accompanying the neutron flux, typically one 422-keV gamma per 20 fast neutrons or about  $3 \times 10^{10}$  neutrons/cm<sup>2</sup> rad(Si), (ii) the open geometry, which allows the placement of large pieces of auxiliary equipment such as ovens, dewars, pressure or vacuum chambers etc. right up to the fast neutron station, (iii) the simple neutron dosimetry based on <sup>7</sup>Be assays, (iv) the point-like nature of the source which generates a fluence with a  $1/r^2$  dependence, and (v) the possibility of using the source with a pulsed beam with a 0.25 ns burst duration. Our station shares with fast burst reactors the advantage of the virtual absence of slow neutrons ( $E < 10$  keV), with a slow-to-fast ratio under 0.1%.

### II. SOURCE DESCRIPTION

#### A. The nuclear reactions

The cycle of isotopes involved is shown in Fig. 1 [1]. Protons incident upon <sup>7</sup>Li transform it into <sup>8</sup>Be, which decays to <sup>7</sup>Be, via neutron emission. The decay may proceed to the ground state of <sup>7</sup>Be, involving  $n_0$ , the first neutron group, or it may lead to the first excited state of <sup>7</sup>Be, via  $n_1$ , the second neutron group. The relative intensity of  $n_0$  and  $n_1$  is a function of the incident proton energy. The percentages given in Fig. 1 refer to 4-MeV protons incident upon a thick Li target.

The gamma transitions following  $n_1$  are the source of the gamma radiation which accompanies the neutron fluence. The gamma radiation is isotropic in space whereas the neutron fluence is peaked in the forward direction.

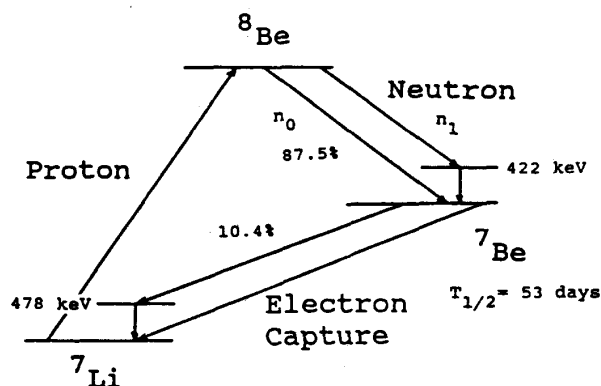


Figure 1. Nuclear reactions with  ${}^7\text{Li}$ .

Hence the gamma-to-neutron ratio (1:20) differs from the  $n_1$ -to- $(n_1 + n_0)$  ratio (1:8).

Beryllium-7 is radioactive [1], it decays back to  ${}^7\text{Li}$  with a half-life of 53 d. Of all disintegrations 10.4% proceed via the first excited state of  ${}^7\text{Li}$  generating a 478-keV gamma ray. The 10.4% figure has been questioned recently; yet eight independent measurements have confirmed it [2].

Note that every neutron emitted from the target leaves a  ${}^7\text{Be}$  nucleus behind. The number of these nuclei can be obtained by measuring the  ${}^7\text{Be}$  decay rate via the 478-keV gamma radiation. In fact this measurement may be repeated within a few weeks, should there be any doubt about its initial correctness.

We have made it a rule, at Lowell, not to use a Li target for more than 24 hours. With this precaution the contribution of the 478-keV gamma ray to the gamma background during the 24 hour neutron irradiation is negligible. We reason as follows: Let the neutron emission rate be  $R$ , then at the end of  $t = 1$  day there are  $Rt$  nuclei of  ${}^7\text{Be}$ ; the emission rate of 422-keV gamma is  $R/8$  and that of the 478-keV line is  $0.104Rt/\tau$  where  $\tau = 76.9$  days is the mean life of  ${}^7\text{Be}$ . It follows that the emission rate ratio (478-keV gamma)/(422-keV gamma) is  $\approx 0.01$  so that the build-up of the 478 keV is negligible.

### B. Target geometry

Protons from the Van de Graaff accelerator are energy-analyzed, collimated, and are incident upon a metallic lithium target in the vacuum of the beam pipe. The lithium target is mounted in a stainless steel planchet, as shown in Fig. 2.

The planchet diameter is 2.54 cm; the metallic Li layer is about 0.1 cm thick. This thickness exceeds the range of 4-MeV protons in Li.

The planchet may be readily replaced to facilitate  ${}^7\text{Be}$  assaying. Typical proton currents are 20 to 25  $\mu\text{A}$  with the proton energy usually set to 4 MeV. These conditions correspond to a target power input from 80 to 100 W; water cooling was found adequate to keep Li metal from melting. One single O-ring is used to provide water-air, air-vacuum, and vacuum-water seals; it is subject to a heavy radiation dose. To avoid leaks the O-ring is replaced whenever a new planchet is installed.

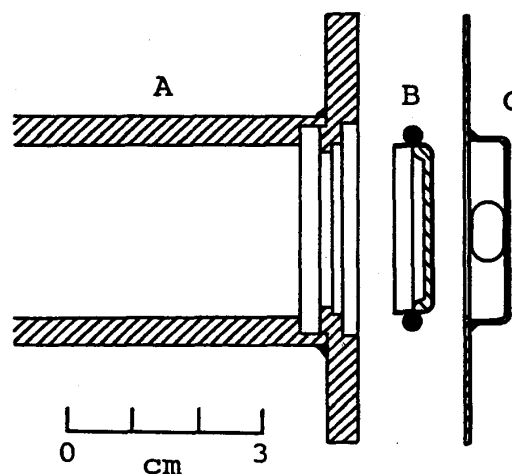


Figure 2. An exploded view of the target components. A: The beam pipe. B: The target planchet loaded with Li and carrying an O-ring. C: The cooling sleeve.

The entire front end is insulated electrically from the collimator and from the accelerator beam line. This permits us to measure proton target current, and by integration, the accumulated charge, which we designate by  $Q$ . For this purpose the current is passed through a 10-k $\Omega$  standard resistor and the resultant voltage drop is fed to a voltage-to-frequency converter. The output of this unit drives a cycle counter where each count represents  $10^{-9}$  coulomb.

The lithium target  ${}^7\text{Be}$  activity may reach 20 mCi after a 24-hour run, so safe radiological procedures are employed in target maintenance. A description of the target making process has been published [3] and may be consulted for details.

### III. NEUTRON GENERATION

#### A. Theory

As protons penetrate the Li target they quickly dissipate their energy by atomic excitation and ionization. Only about one proton in 2000 will generate a neutron and the generation of two neutrons by one proton is negligible under the conditions we describe. For applications it is important to know the energy and the directional distributions of the neutrons produced. Three processes govern these distributions. We review them briefly; a more detailed discussion is available [4]. (i) The reaction kinematics determines the neutron energy once proton energy and neutron emission angle are specified. Most nuclear physics textbooks discuss kinematics of p-n reactions in detail, see, e.g. Ref. 5.

(ii) The stopping power,  $\epsilon$ , of lithium for protons is defined as

$$\epsilon = (-1/C_L)(dE_p/dx) \quad (1)$$

Here  $E_p$  is the proton energy;  $x$  is the path length coordinate in the target, with  $x=0$  at the Li surface;  $C_L$  is the atomic concentration of lithium.

The stopping power  $\epsilon$  represents the rate of energy loss of a proton as it penetrates lithium. If we specify  $E_p$  and  $dE_p$  then  $(dE_p/\epsilon) = C_L dx$  is the number of Li atoms per area which a proton encounters as its energy decreases from  $E_p + dE_p$  to  $E_p$ . Experimental results for have been reviewed by Whaling [6].

(iii) The differential cross section for neutron emission  $d\sigma/d\omega$  is a function of the proton energy and of the neutron emission angle,  $\theta$ . This function determines the probability for emission of a neutron in a specified direction. The extensive literature on measurements of the  ${}^7\text{Li}(p,n){}^7\text{Be}$  reaction has been reviewed by Liskien and Paulsen [7].

We can combine (ii) and (iii) and find that

$$F = (d\sigma/d\omega) (dE_p/\epsilon) \quad (2)$$

is the function which governs emission of a neutron within a neutron energy interval  $dE_n$  into a direction specified by  $\theta$ . The three processes are illustrated in Fig. 3.

The preceding discussion forms the basis for a computer code written in our laboratory to determine neutron fluences and spectra [4]. Results shown in Figs. 4-6 are obtained with this code. Figure 4 is a histogram portraying the neutron energy distribution. The structure present in  $d\sigma/d\omega$  near  $E_p = 2.5$  MeV (Fig. 3) is reflected in the peak near  $E_n = 0.5$  MeV. The upper end of the neutron energy distribution is determined by the energy of the protons as they reach the Li surface; this end point may be

raised or lowered by changing the proton energy.

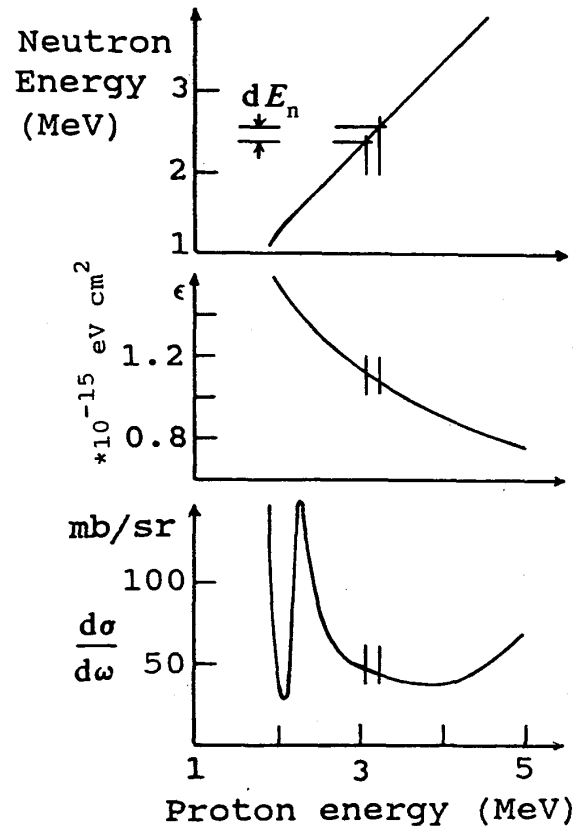


Figure 3. These three graphs represent from top to bottom, the reaction kinematics, the stopping power  $\epsilon$ , and the reaction cross section  $d\sigma/d\omega$ , all as functions of the proton energy.

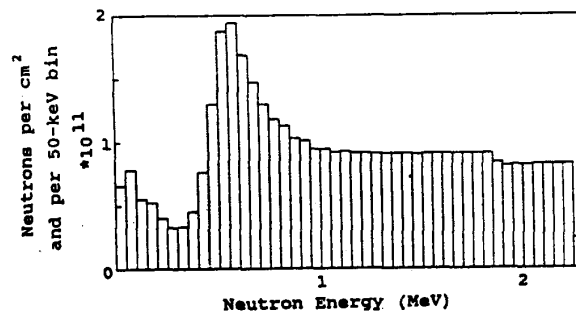


Figure 4. A calculated neutron energy histogram.

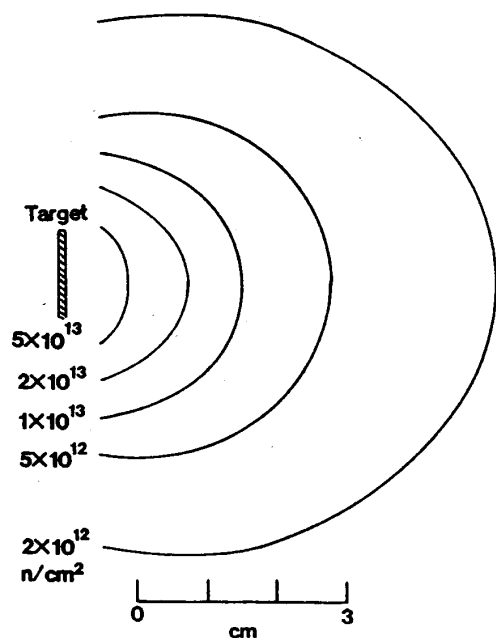


Figure 5. Calculated neutron isofluence contours for a 90-min., 20- $\mu$ A, 4-MeV exposure.

Figure 5 shows isodose contours. Neutrons carry a substantial fraction of the protons linear momenta; this causes the enhancement of neutron emission in the forward direction. Figure 6 shows the radial dependence of the neutron fluence, in the forward direction. Except for distances close to the target the fluence decreases as  $1/r^2$ .

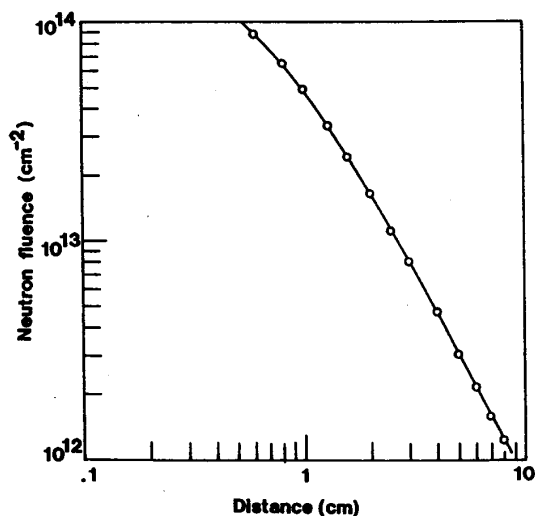


Figure 6. The calculated neutron fluence in the forward direction as a function of target distance for a 90-min., 20- $\mu$ A, 4-MeV exposures.

For close distances one may use the approximation for the fluence  $\phi$

$$\phi \propto \ln(1+R^2/r^2) \quad (3)$$

where  $R$  is the target radius.

Computer code MURI does not include corrections for neutron absorption in the target planchet, in the cooling water or in the cooling sleeve because the code was written before the present target geometry had been established. The applicable corrections, either to the fluence or to the spectrum, are small because about 82% of all neutrons emitted in the forward direction do not interact with the target hardware. We review neutron attenuation in the appendix and we estimate that there is a fluence attenuation of 4.2%; in addition there is a spectrum distortion with a 9% reduction at the high energy end and an increase at the low energy end.

It is possible to reduce the attenuation and the distortion by spray cooling the target planchet. In this case the coolant thickness is less than 1 mm and the cooling sleeve is eliminated. Neutron fluence attenuation is 1.9% and the spectrum distortion is reduced by a factor of four. This form of cooling has been used in the time-of-flight measurements reported in IV-D.

### B. Measurements

In this section we describe routine measurements of the total number of neutrons produced by a target and we review one measurement of the neutron fluence in the forward direction. The total neutron production of a target is equal to the number of  $^7\text{Be}$  nuclei it contains. This figure is obtained from the emission rate of 478-keV gamma rays, which follow the decay of  $^7\text{Be}$ , see Fig. 1. We use a cooled Ge detector for these measurements. To determine its detection efficiency we recorded the spectrum of a multiple gamma-ray source and obtained efficiencies for eleven gamma or x-ray lines, between 88 keV and 1836 keV. Inspection of the result showed that there is a linear relationship between  $\ln \eta$  ( $\eta$  = efficiency) and  $\ln E_\gamma$  in the energy interval from 397 to 661 keV. To confirm this appearance we used a Standard Reference Material Source [8] to measure the detector efficiency for four gamma lines between 428 and 601 keV and we approximate the efficiency by

$$\ln \eta = a \ln E_\gamma + b \quad (4)$$

using a least square fit technique. The fit residual indicates a relative standard deviation of one measurement of 0.7%, in good agreement with statistical uncertainties of four measurements which vary from 0.4% to 0.7%.

In view of this result we have used the approximation (4) in all subsequent efficiency determinations. We have also included a fifth gamma line, at 636 keV to the set to be fitted by Eq. (4). The fit gives us the detector efficiency at 478 keV, the energy of the gamma line in the  $^7\text{Be}$  decay.

Normally the reference standard is placed at a distance of 15.2 cm from the outside of the detector housing. This distance is far too close for most  $^7\text{Be}$  samples with their milliCurie activities. We therefore place  $^7\text{Be}$  samples at approximately 220 cm and compute the detection efficiency for this distance using the inverse square law. This requires knowledge of the position where  $r=0$ , i.e., the average position of the first interaction of a gamma ray entering the germanium. We obtain this datum as follows.

The separation between the detector surface and the outside of the detector housing is 0.75 cm. The average depth of the first interaction is equal to the inverse of the linear gamma absorption coefficient in Ge at 478 keV. This coefficient is known [9]. Its inverse is 2.22 cm so that the interaction center is located at  $r_0=2.97$  cm behind the outside detector housing.  $r_0$  was added to all distance measurements before the  $1/r^2$  relation was used.

Efficiency determinations remained "valid" for about four weeks; after that time they were considered "obsolete" and had to be repeated.

We denote by  $N$  the actual number of  $^7\text{Be}$  atoms in a target. To obtain  $N$  is not difficult once the 478-keV gamma emission rate is known because the pertinent branching ratio and the  $^7\text{Be}$  mean life are well known [1]. Typical values of  $N$  range from  $2 \times 10^{14}$  to  $5 \times 10^{15}$ .

With  $N$  and  $Q$  we have the means to check our computer code MURI. We have calculated the ratio  $R$ ,

$$R = N/Q \quad (5)$$

for each target and we have computed the average value of  $R$  for two groups of targets, each used during a  $\approx 18$  months period. Numbers obtained from MURI indicate  $R=3.3484$  n/fC. This datum must be corrected since our targets contain  $^6\text{Li}$  and  $^7\text{Li}$ . Since the isotopic compositions of commercial Li vary [1] we designed a procedure to measure the isotopic concentration of our samples [10] and we found close agreement with the recommended values of 7.5 at% of  $^6\text{Li}$  and 92.5 at% of  $^7\text{Li}$ . This leads to a corrected value for  $R$ ,

$$R_{\text{theory}} = 3.0977 \text{ n/fC} \quad (6)$$

This number should be compared with the experimental average shown in Table I. The good agreement strengthens

our confidence in code MURI. In addition, the magnitude of the data scatter of  $R$  from run to run suggests that we can determine  $N/Q$  with a 3.3% accuracy.

Table I.  
Measured and calculated  $N/Q$

Number of runs	$\langle N/Q \rangle$ measured [n/fC]	$N/Q$ Theory [n/fC]	Percent Difference	Relative Standard Deviation (one run)
25	3.1079	3.0997	0.27%	4.9%
19	3.0732	3.0997	0.82%	3.3%

There is one other experiment we should report at this time. To measure the neutron fluence in the forward direction we have placed a metallic nickel disk in close proximity of the neutron target. (The distance from the disk to the lithium surface was 0.75 cm.) The disk had a mass of 4.5913 g and contained  $3.197 \times 10^{22}$  atoms of  $^{58}\text{Ni}$ . This disk was irradiated for 200 minutes. The reaction  $^{58}\text{Ni}(n,p)^{58}\text{Co}$  took place and we could determine the number of  $^{58}\text{Co}$  atoms in two ways: (i) We measured the emission rate of the 811-keV gamma line, which follows the decay of  $^{58}\text{Co}$ . This leads to  $1.844 \times 10^{10}$  atoms of  $^{58}\text{Co}$ , and to a  $^{58}\text{Co}$ -to- $^{58}\text{Ni}$  ratio of  $5.768 \times 10^{-13}$ . (ii) We used the  $^7\text{Be}$  assay and code MURI to determine the neutron fluence reaching the nickel foil.

In this second approach we used a special version of MURI which provides neutron energy spectra weighted with the  $^{58}\text{Ni}(n,p)^{58}\text{Co}$  cross section as given by McLane et al. [11]. The disk was subdivided into one circular center portion and ten annular regions and MURI was run for the eleven regions to account for the spatial variations of the neutron fluence. This approach leads to  $2.121 \times 10^{10}$  atoms of  $^{58}\text{Co}$ . The attenuation of neutrons in lithium, in water, and in copper should be taken into account. Using appropriate total cross sections we obtain a neutron attenuation factor of 0.859 which would lead to a calculated number of Co atoms of  $1.826 \times 10^{10}$ , and to a  $^{58}\text{Co}$ -to- $^{58}\text{Ni}$  ratio of  $5.712 \times 10^{-13}$ . This attenuation factor is certainly too large since it does not account for neutrons which are scattered with some energy loss, but which still reach the Ni disk. We are considering using a more elaborate code for the analysis of this and other similar experiments. At present we estimate that experimental and calculated data agree to within 8%.

#### IV. APPLICATIONS

In this section we review several examples of the use of the Lowell fast neutron facility. The examples

selected illustrate some unique features of our neutron source.

### A. Irradiation of integrated circuits

Sets of fourteen- to sixteen-pin "dip" integrated circuits have been irradiated frequently. Typically ten devices are mounted on an aluminum support shaped to approximate an isodose surface so that all samples receive the same exposure. The distance between this bracket and the lithium target surface is 4.0 cm. When operating with a 4-MeV, 25- $\mu$ A proton beam a fluence of  $4 \times 10^{12}$  n/cm<sup>2</sup> is obtained in one hour; about 24 hours are needed to reach  $10^{14}$  n/cm<sup>2</sup>. Users usually retrieve the samples for testing at fluence levels of  $10^{12}$ ,  $3 \times 10^{12}$ ,  $10^{13}$ ,  $3 \times 10^{13}$ , and  $10^{14}$  n/cm<sup>2</sup>. The higher exposure levels from  $3 \times 10^{13}$  to  $10^{14}$  n/cm<sup>2</sup>, can be achieved in overnight runs. Frequently users interleave two or more sets of devices so that one set may be irradiated while another set undergoes testing.

S. Wilensky [13] has compared the costs of reactor and accelerator neutron irradiations. While the cost per fluence is higher on the accelerator he finds that accelerator radiation effects testing may be less costly, in certain cases, due to the absence of slow neutrons.

### B. Bacteria irradiation

In this example advantage is taken of the strong spatial fluence variation, see Fig. 6. The resistance of *Deinococcus radiodurans* and of *Escherichia coli* bacteria to fast neutron irradiation has been tested. Bacteria on

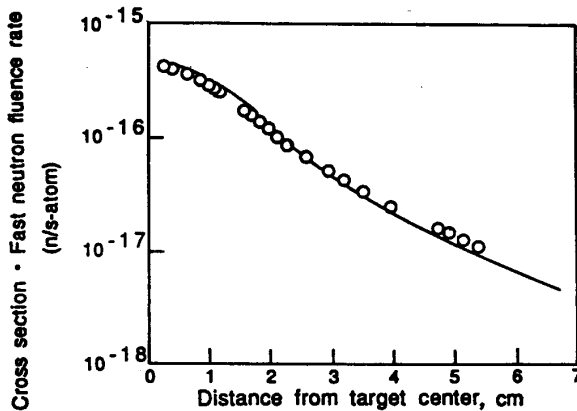


Figure 7. Measured (circles) and calculated (solid line) neutron fluence rates per <sup>115</sup>In atom as determined across a Petri dish as functions of the target distance.

membrane filters were placed on nutrient solutions in Petri dishes. For irradiation a dish was mounted in front of and close to the neutron target so that its symmetry axis

coincided with that of the lithium target. Indium pellets were distributed over an otherwise empty dish for neutron fluence rate determinations. This dish was irradiated to near saturation ( $\approx 24$  hours) and the activity induced in the pellets via the  $^{115}\text{In}(n,n')^{115m}\text{In}$  reaction was measured. Neutron fluence rates deduced from these measurements are shown in Fig. 7 together with a solid line representing calculated data. In this case too, we believe that neutron absorption plays a major role in creating deviations between measured and computed values.

### C. Wafer irradiation

For this third example the near absence of gamma rays was of value and the spatial variation of the neutron fluence contributed to the success. The lack of induced activities permitted the mailing of the irradiated sample within hours after irradiation. A detailed account of the work has been given by A. Reisman et al. [14].

A 4-inch silicon wafer with approximately 220 devices was mounted in front of the neutron target at an angle of 30° to the horizontal so that there was a large change in neutron fluence from one side of the wafer to the other. MURI was again used to compute neutron fluences for each of the 220 devices. Figure 8 shows the minority carrier lifetime as a function of the fast neutron fluence. The dashed line is a fit to the equation

$$\tau = \tau_0 / (1 + bF) \quad (7)$$

where  $F$  is the neutron fluence,  $\tau_0$  the pre-irradiation

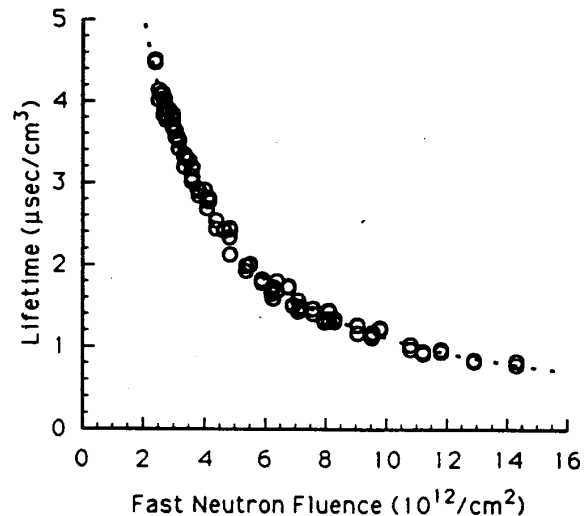


Figure 8. Minority carrier life-times vs. neutron fluences. The dashed curve is a fit to the experimental data from Ref. 14.

lifetime ( $47.4 \mu\text{s}/\text{cm}^3$ ), and  $b = 4.2 \times 10^{-12} \text{ cm}^2$  a degradation parameter determined by the fit. As can be seen the fit of Eq. (7) to the data is excellent.

Reisman and coworkers could not verify the presence of neutron induced positive charges nor of neutral traps in gate insulators. The small positive charge buildup observed could be accounted for fully by the small amount of gamma-ray absorption in the gate oxide.

This example illustrates some advantages to be gained by wafer irradiation. An irradiation of this type covers a range of neutron fluences, dosimetry is simplified, sample homogeneity is assured and abundant results are obtained.

#### D. Time-of-flight measurements

In this application we describe the use of a subnanosecond pulsed beam. The determination of the detection efficiency of a neutron detector used in fast neutron scattering experiments is a time consuming task

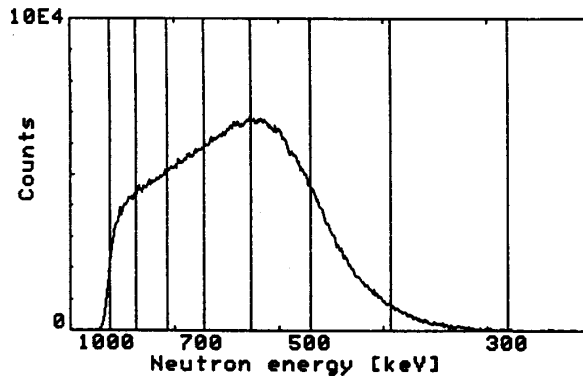


Figure 9. A neutron time-of-flight spectrum.

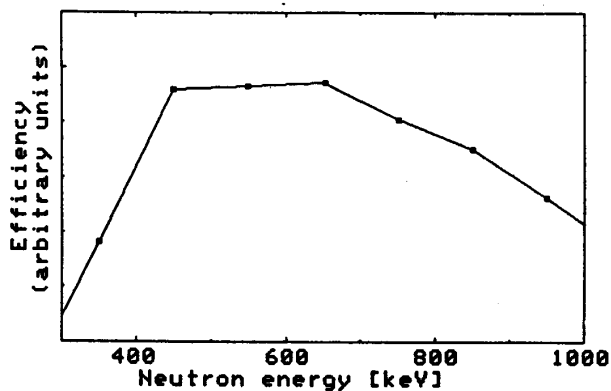


Figure 10. The efficiency of a neutron detector as described from MURI and from the data of Fig. 9.

and, in consequence, is not carried out as often as desirable. To simplify this determination we produce a short ( $\Delta t \approx 300\text{ps}$ ) burst of neutrons from a thick target and we measure the neutron time-of-flight spectrum as shown in Fig. 9. The proton energy was selected to give a maximum neutron energy of 1000 keV. The neutron time-of-flight spectrum is subdivided into 100 keV-wide energy bins. The actually measured number of neutrons in one bin divided by the computed number of neutrons equals to the detector efficiency, as shown in Fig. 10. The principal advantage of this efficiency determination is its speed; it took less than 10 minutes to measure the spectrum of Fig. 9.

#### V. ACKNOWLEDGMENT

The authors are indebted to Mr. David Shaw for his expert maintenance of the Van de Graaff accelerator. Members of the Neutron Scattering group at Lowell (LTI) have helped us in many phases of this work. The referees of this paper are to be thanked for their numerous valuable suggestions.

#### VI. APPENDIX

##### Neutron Attenuation

In this appendix we estimate the effects of neutron interactions with target materials. These materials are listed in Table II. It is convenient to consider separately neutron interactions with the heavier elements, Li, O, Cr, Fe, Ni, and Cu, and with hydrogen.

Table II.  
Target materials.

Material	Thickness (mm)	Fraction of neutrons scattered in the material
Li	1.0	0.9%
Planchet	0.38	1.1%
Water (O)	3.83	3.8%
Water (H)	3.83	9.0%
Cooling sleeve	0.91	2.6%

Neutron interactions with heavier elements are primarily elastic scattering processes which change neutron directions of motion without changing their energies appreciably. Hence the loss of neutron fluence in one direction due to outscattering is compensated in part by in-scattering of neutrons which moved in different directions

originally. This compensation does not apply to backscattered neutrons due to the absence of scattering material in that direction.

If we assume that the pertinent elastic scattering cross sections are isotropic (an approximation acceptable in view of the smallness of the overall attenuation) then about one half of the interacting neutrons are lost due to elastic scattering. This would reduce the contribution of heavier elements to the attenuation to one half of 8.4% or 4.2%. This reduction would cover the entire energy spectrum in an approximately uniform way.

The strong resonance in the Li total and elastic cross sections at a neutron energy of 260 keV is of less concern since the neutron spectrum has a minimum at this very energy, a convenient coincidence.

Interactions with hydrogen are different. Again the interactions are elastic scattering processes, but since the hydrogen and neutron masses are nearly equal there is no neutron backscattering and there is a large energy transfer from the neutron to the struck hydrogen nucleus. A detailed analysis shows that a neutron with energy  $E_n$  when colliding with a proton will lose energy between zero and  $E_n$  with nearly equal probability.

If we assume again that in-scattering compensates for out-scattering then interactions with hydrogen do not reduce the number of neutrons but change the energy spectrum. The largest reduction of 9% occurs at the upper end of the energy spectrum; lower energy neutrons will appear less attenuated. Neutrons at 800 keV will appear unchanged and there will be an increase of neutron fluence at lower energies.

## VII. REFERENCES

- [1] C. Michael Lederer and Virginia Shirley, *Table of Isotopes*, New York: Wiley, 1978, pp. 3-4.
- [2] S. A. Fisher and R. I. Hershberger, "Branching ratios for EC decay of  $^7\text{Be}$  and  $^{51}\text{Cr}$ ," *Nucl. Phys. A*, vol. 423, pp. 121-129, 1984.
- [3] G. H. R. Kegel, "Fast neutron generation with a type CN Van de Graaff accelerator," *Nucl. Instr. and Meth. in Phys. Res. B*, vol. 40/41, pp. 1165-1168, 1989.
- [4] Gunter H. R. Kegel, "Fluences and energy spectra of fast neutrons from a proton irradiated thick lithium target," *Comp. Phys. Communic.*, vol. 36, pp. 321-336, 1985.
- [5] Robley D. Evans, *The Atomic Nucleus*, New York: McGraw-Hill, 1955, pp. 408-440.
- [6] W. Whaling, *Handbuch der Physik*, vol. XXXIV, Berlin: Springer, 1958.
- [7] Horst Liskien and Arno Paulsen, "Neutron production cross sections and energies for the reactions  $^7\text{Li}(p,n)^7\text{Be}$  and  $^7\text{Li}(p,n)^7\text{Be}^*$ ," *Atomic Data and Nuclear Data Tables*, vol. 15, pp. 15-84, January 1975.
- [8] *Standard Reference Material 4275-174*, National Bureau of Standards, Washington, D.C., June 1981.
- [9] J. B. Marion and F. C. Young, *Nuclear Reaction Analysis, Graphs and Tables*, Amsterdam: North Holland Publishing Co., 1968, p. 65.
- [10] Causon K. C. Jen and Gunter H. R. Kegel, "Measurement of the lithium isotopic concentration," *Nucl. Instr. and Meth. in Phys. Res. B*, vol. 62, pp. 242-246, 1991.
- [11] Victoria McLane, Charles L. Dunford and Philip F. Rose, *Neutron Cross Sections*, vol. 2, Boston: Academic Press, 1988.
- [12] B. T. Ahlport and S. L. Anderson, "Easy Prediction of Degradation in Transistor Current Gain over Large Range of Operating Current," *IEEE Transactions on Nuclear Science*, vol. NS-31, pp. 1417-1422, 1984.
- [13] Samuel Wilensky, "A comparison of reactor and accelerator sources for neutron effects testing," *Jour. Electronic Mat.*, vol. 21, pp. 689-691, July 1992.
- [14] A. Reisman, M. Walters, and G. H. R. Kegel, "Neutron irradiation of insulated gate field effect transistors," *Jour. Electronic Mat.*, vol. 20, pp. 935-938, 1991.